(Received 28 April 2026, Accepted 17 June 2026, Scheduled 3 August 2026)

# Volume Surface Integral Equation Method with Finite-Gap Lumped-Port Model for EM Radiation by Composite Metallic-Dielectric Structures

Chun-Ying Zhao[1], Zi-Qiang Wu[2], Shi-Chao Zeng[1], Qin-Lei Zhang[1], Long-Jian Zhou[2], and Qiang-Ming Cai[2,*]

[1] *Chengdu Spaceon Technology Development Co.,Ltd., Chengdu, China*
[2] *School of Information and Control Engineering, Southwest University of Science and Technology, Mianyang, China*

**ABSTRACT:** A novel finite-gap lumped-port model is presented to improve the accuracy of the volume surface integral equation (VSIE) solver for electromagnetic (EM) radiation from composite metallic-dielectric structures. This port model is implemented by modifying the traditional method of moments (MoM) solution to use a novel divergence-conforming testing function at the gap as well as half-basis functions connected across the gap, where a small gap region in the domain of analysis is linked to the lumped-circuit voltage/current source. Then, a hybrid multilevel fast multipole algorithm with multilevel accelerated Cartesian expansion algorithm (MLFMA-MLACEA) is adopted to enhance the capability of this VSIE-based finite-gap lumped-port model for electrically large and multi-scale EM radiation problems. Numerical results are provided to demonstrate the accuracy and efficiency of this VSIE method.

## 1. INTRODUCTION

The electromagnetic (EM) radiation from metallic targets, composite metallic-dielectric (CMD) structures, electrically large objects, and multi-scale configurations is of great significance for electromagnetic compatibility (EMC), target detection, EM communications, and other related applications. To accurately extract network parameters or analyze the EM radiation of a given target, various lumped-port models have been developed to represent localized excitations within integral equation (IE) methods [1–6]. Among them, the delta-gap model is the most widely used due to its simplicity: it approximates the uniform electric field over an infinitesimal gap and is straightforward to implement, offering acceptable accuracy for many problems. However, the delta-gap model inherently introduces numerical errors, as the infinitesimal gap requires artificial connecting pieces on both sides, which cause deviations from the physically correct solution. To circumvent this issue, the finite-gap lumped-port model was proposed [7, 8]. Nevertheless, for simple metallic antennas, the delta-gap model remains sufficiently accurate [7]; the finite-gap model becomes essential only when higher fidelity or more complex geometries are involved.

For CMD structures, the metallic part can be modeled by the surface integral equation (SIE) [9–11], while the dielectric part, often inhomogeneous, is better handled by the volume integral equation (VIE) [12, 13]. The combination of VIE and SIE is known as the volume-surface integral equation (VSIE) [14–16]. In this paper, we propose a novel VSIE scheme with a finite-gap lumped-port model for the simulation of CMD structures. The proposed port model is implemented by modifying the traditional VSIE solution based on the delta-gap model to incorporate a novel divergence-conforming testing function at the gap, as well as half-basis functions connected across the gap. It is worth noting that this finite-gap lumped-port model has been utilized in an SIE framework for pure metallic structures [17, 18]. However, different from previous works, to the best of our knowledge, this model is applied to the VSIE for the first time. Given that VSIE has a broader range of applicability, this extension is both important and valuable. In our scheme, the VSIE is discretized using the Rao-Wilton-Glisson (RWG) [9] and Schaubert-Wilton-Glisson (SWG) [12] basis functions defined on planar elements. However, this straightforward discretization leads to a large number of unknowns when dealing with electrically large or multi-scale objects. To address this computational challenge, we employ the hybrid MLFMA-MLACEA method [19–21] to accelerate the solution of the VSIE. In addition, normalized basis functions (NBF) [22] and sparse approximate inverse (SAI) [23] techniques are used to improve the conditioning of the impedance matrices, further enhancing numerical stability.

The main contribution of this work is the integration of a finite-gap lumped-port model into a VSIE framework for the accurate analysis of EM radiation from CMD structures. Unlike previous studies that applied the finite-gap model only to simple metallic antennas, our method rigorously accounts for inhomogeneous dielectric material and finite physical gap size, thereby eliminating the spurious connecting pieces inherent in the delta-gap model. This leads to more reliable network parameter extraction, especially for electrically large and multi-scale prob-

* Corresponding author: Qiang-Ming Cai (qmcai@swust.edu.cn).

lems where the delta-gap approximation may fail. The hybrid MLFMA-MLACEA acceleration ensures that the resulting VSIE system remains computationally tractable, while the improved preconditioning guarantees fast convergence.

The remainder of this paper is organized as follows. Section 2 outlines the basic theories of the VSIE and the half-RWG model, and details the implementation of the finite-gap lumped-port excitation within the VSIE framework. Section 3 presents numerical results that demonstrate the accuracy, efficiency, and robustness of the proposed method in a variety of test cases, including composite structures with electrically large dimensions and fine geometric features. Finally, Section 4 concludes the paper with a discussion of potential extensions.

## 2. THEORY

### 2.1. Volume Surface Integral Equation (VSIE)

Consider an arbitrarily shaped three-dimensional composite structure consisting of a metallic surface $S$ and an inhomogeneous dielectric object $V$, as illustrated in Fig. 1. The structure is immersed in a homogeneous background medium with permittivity $\varepsilon_b$ and permeability $\mu_b$. Within the dielectric region $V$, an equivalent complex permittivity $\varepsilon_c = \varepsilon - j\omega\sigma/\omega$ is assumed, where $\varepsilon$ and $\sigma$ denote the permittivity and conductivity, respectively. The structure is illuminated by a time-harmonic $(e^{j\omega t})$ wave with incident electric field $\mathbf{E}^{inc}$ and magnetic field $\mathbf{H}^{inc}$, originating from outside.

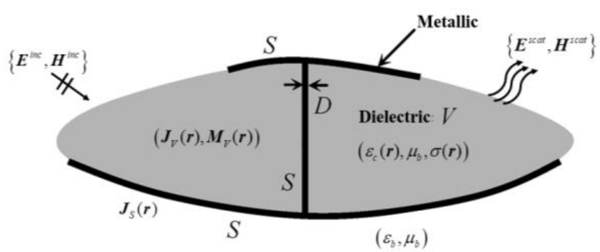


**FIGURE 1**. Geometry of composite metallic-dielectric structure.

The scattered electromagnetic field $\mathbf{E}^{scat}$ is generated by the equivalent surface current $\mathbf{J}_S$ and $S$ and the equivalent volume currents $\mathbf{J}_V$ and $V$. The fields can be formulated as

$$\mathbf{E}_S^{scat} = -jk_b\eta_b\mathcal{L}_s\{\mathbf{J}_S\} - jk_b\eta_b\mathcal{L}_v\{\mathbf{J}_V(\mathbf{r})\}, \ \mathbf{r} \in S \quad (1)$$

$$\mathbf{E}_V^{scat}(\mathbf{r}) = -jk_b\eta_b\mathcal{L}_s\{\mathbf{J}_S(\mathbf{r})\} - jk_b\eta_b\mathcal{L}_v\{\mathbf{J}_V(\mathbf{r})\}, \mathbf{r} \in V \quad (2)$$

where $k_b$ and $\eta_b$ denote the wave number and intrinsic impedance of the background medium, respectively. The operators $\mathcal{L}_\mathcal{D}\{\mathbf{X}\}$ ($\mathcal{D} = S/V$) is defined as

$$\mathcal{L}_\mathcal{D}\{\mathbf{X}(\mathbf{r})\} = \int_\mathcal{D} \mathbf{X}(\mathbf{r}')G(\mathbf{r},\mathbf{r}')d\mathbf{r}' - (jk_b)^{-2}\nabla\int_\mathcal{D} G(\mathbf{r},\mathbf{r}')\nabla'\cdot\mathbf{X}(\mathbf{r}')d\mathbf{r}' \quad (3)$$

where $G(\mathbf{r},\mathbf{r}') = e^{-jk_bR}/(4\pi R)$ is the Green's function in the homogeneous medium, and $R$ is the distance between the field point $\mathbf{r}$ and source point $\mathbf{r}'$.

The electric fields on the metallic surface $S$ satisfy the following boundary conditions [3–6], and we have the following electric-field integral equation (EFIE):

$$0 = \hat{\mathbf{n}} \times \left(\mathbf{E}^{inc}(\mathbf{r}) + \mathbf{E}_V^{scat}(\mathbf{r}) + \mathbf{E}_S^{scat}(\mathbf{r})\right), \quad \mathbf{r} \in S \quad (4)$$

where $\hat{\mathbf{n}}$ is the outward unit normal vector on $S$. Inside the dielectric region $V$, the total electric field is

$$\mathbf{E}(\mathbf{r}) = \mathbf{E}^{inc}(\mathbf{r}) + \mathbf{E}_V^{scat}(\mathbf{r}) + \mathbf{E}_S^{scat}(\mathbf{r}), \quad \mathbf{r} \in V \quad (5)$$

Based on the volume equivalent principle [9], we have the following volume electric-field integral equation (VEFIE):

$$\mathbf{J}_V(\mathbf{r}) = j\omega\zeta(\mathbf{r})\varepsilon_c(\mathbf{r})\mathbf{E}(\mathbf{r}) = j\omega\zeta(\mathbf{r})\mathbf{D}(\mathbf{r}) \quad (6)$$

$$\zeta(\mathbf{r}) = \frac{\varepsilon_c(\mathbf{r}) - \varepsilon_b}{\varepsilon_c(\mathbf{r})}, \quad \mathbf{D}(\mathbf{r}) = \varepsilon_c(\mathbf{r})\mathbf{E}(\mathbf{r}) \quad (7)$$

where $\mathbf{D}(\mathbf{r})$ is the electric flux density vector, and $\zeta(\mathbf{r})$ is the ratio of electric contrast. By combining EFIE (4) and VEFIE (6), the VSIE is given by

$$\hat{\mathbf{n}}\times\Big[\mathcal{L}_s\{\mathbf{J}_s(\mathbf{r})\}+\mathcal{L}_v\{\mathbf{J}_v(\mathbf{r})\}\Big] = \frac{\hat{\mathbf{n}}\times\mathbf{E}^{inc}(\mathbf{r})}{jk_b\eta_b}, \quad \mathbf{r} \in S \quad (8a)$$

$$\mathcal{L}_s\{\mathbf{J}_s(\mathbf{r})\} + \frac{1}{jk_b\eta_b}\mathbf{E}(\mathbf{r}) + \mathcal{L}_v\{\mathbf{J}_v(\mathbf{r})\} = \frac{\mathbf{E}^{inc}(\mathbf{r})}{jk_b\eta_b}, \quad \mathbf{r} \in V \quad (8b)$$

### 2.2. Current Modeling and Matrix Equation of VSIE

In this section, $\mathbf{J}_V$ and $\mathbf{J}_S$ are expanded using the RWG $\mathbf{F}_n^S$ and SWG basis functions $\mathbf{F}_n^V$, defined on triangles and tetrahedra, respectively. Thus, we have:

$$\mathbf{D}(\mathbf{r}) = \eta_b\varepsilon_b\sum_{n=1}^{N_V} I_n^V\mathbf{F}_n^V(\mathbf{r}) \quad (9)$$

$$\mathbf{J}_S(\mathbf{r}) = \sum_{n=1}^{N_S} I_n^S\mathbf{F}_n^S(\mathbf{r}) \quad (10)$$

where $N_V/N_S$ is the number of the SWG/RWG basis, and $I_n^V/I_n^S$ is the unknown expansion coefficients of $\mathbf{F}_n^V/\mathbf{F}_n^S$. Substituting (9) and (10) into (8), and testing with appropriate weighting functions, we obtain the matrix equation of the VSIE:

$$\begin{bmatrix}\mathbf{Z}_{SS} & \mathbf{Z}_{SD}\\ \mathbf{Z}_{DS} & \mathbf{Z}_{DD}\end{bmatrix}\begin{bmatrix}\mathbf{I}_S\\ \mathbf{I}_D\end{bmatrix} = \begin{bmatrix}\mathbf{V}_S\\ \mathbf{V}_D\end{bmatrix} \quad (11)$$

where the submatrix $\mathbf{Z}_{AB}$ (with $A, B \in \{S, D\}$) represents the contribution of sources in domain $B$ to the field in domain $A$. The vector $\mathbf{I}_A$ denotes the unknown coefficients, and $\mathbf{V}_A$ is the excitation column matrix.

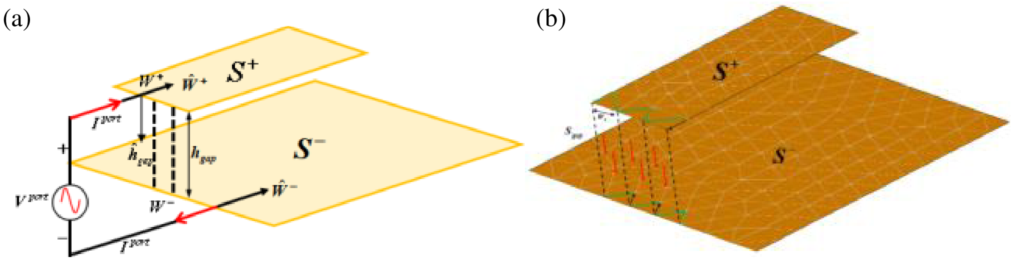


**FIGURE 2**. The finite-gap model. (a) A current/voltage source connected to an electromagnetically small gap that separates two portions of a metallic surface and (b) the port currents discretized by half-RWG basis functions.

### 2.3. Finite-Gap Lumped-Port Model

In this paper, three types of excited sources, i.e., finite-gap voltage source, finite-gap current source, and finite-gap mixed source, will be considered. Note that this finite-gap lumped-port model has been utilized in the SIE framework for pure metallic structures [17, 18]. However, different from previous works, to the best of our knowledge, this model is applied to the VSIE for the first time. Given that VSIE has a broader range of applicability, this extension is both important and valuable. As shown in Fig. 2, a finite-gap current model is displayed, where two portions of the surface $S$ are separated by an electromagnetically small gap of height $h$. The surface is assumed to be excited by a time-harmonic lumped current source $I^{port}$ whose terminals are connected to the two portions $S^+$ and $S^-$ in the gap.

To solve this problem, $S$ is meshed using triangular patches with a constraint on the patches at the port: each patch with an edge at the gap is required to have a matching patch with an equal-length edge on the other side of the gap. The metallic current $\mathbf{J}_S$ is approximated using two types of basis functions: standard RWG basis functions defined on connected pairs of patches are used for $\mathbf{J}_S$ away from the gap and half-RWG basis functions on disconnected pairs of patches are used for the $\mathbf{J}_S$ entering/leaving the port (Fig. 2(b)), i.e.,

$$\mathbf{J}_S(\mathbf{r}) = \sum_{n=1}^{N'_S} I_n^S \mathbf{F}_n^S(\mathbf{r}) + \sum_{n=N'_S+1}^{N'_S+N_{port}} I_n^S \mathbf{F}_n^{S,P}(\mathbf{r}) \tag{12}$$

where $N_S = N'_S + N_{port}$, and $N_{port}$ is the total number of unknowns of half-RWG basis functions on disconnected pairs of patches. Thus, (11) can be expressed as

$$\begin{bmatrix} \mathbf{Z}^{S,S}_{N'_S\times N'_S} & \mathbf{Z}^{S,P}_{N'_S\times N_{port}} & \mathbf{Z}^{S,V}_{N'_S\times N_V} \\ \mathbf{Z}^{P,S}_{N_{port}\times N'_S} & \mathbf{Z}^{P,P}_{N_{port}\times N_{port}} & \mathbf{Z}^{P,V}_{N_{port}\times N_V} \\ \mathbf{Z}^{V,S}_{N_V\times N'_S} & \mathbf{Z}^{V,P}_{N_V\times N_{port}} & \mathbf{Z}^{V,V}_{N_V\times N_V} \end{bmatrix} \begin{bmatrix} \mathbf{I}^S_{N'_S} \\ \mathbf{I}^P_{N_{port}} \\ \mathbf{I}^V_{N_V} \end{bmatrix} = \begin{bmatrix} \mathbf{0} \\ \mathbf{V}_{N_{port}} \\ \mathbf{0} \end{bmatrix} \tag{13}$$

where $N_V$ is the total number of unknown quantities of the electromagnetic medium; $\mathbf{V}_{N_{port}}$ represents the unknown voltage at the port; and $\mathbf{I}^P_{N_{port}}$ $(I^P_k = I_{port}/\sum_{k=1}^{N_{port}} w_k)$ is the excitation value of the current source $I_{port}$. Expanding (13), we obtain the system of equations:

$$\mathbf{Z}^{S,S}_{N'_S\times N'_S}\cdot\mathbf{I}^S_{N'_S} + \mathbf{Z}^{S,P}_{N'_S\times N_p}\cdot\mathbf{I}^P_{N_P} + \mathbf{Z}^{S,V}_{N'_S\times N_V}\cdot\mathbf{I}^V_{N_V} = \mathbf{0} \tag{14}$$

$$\mathbf{Z}^{P,S}_{N_p\times N'_S}\cdot\mathbf{I}^S_{N'_S} + \mathbf{Z}^{P,P}_{N_p\times N_p}\cdot\mathbf{I}^P_{N_P} + \mathbf{Z}^{P,V}_{N_p\times N_V}\cdot\mathbf{I}^V_{N_V} = \mathbf{V}_{N_P} \tag{15}$$

$$\mathbf{Z}^{V,S}_{N_V\times N'_S}\cdot\mathbf{I}^S_{N_S} + \mathbf{Z}^{V,P}_{N_V\times N_p}\cdot\mathbf{I}^P_{N_P} + \mathbf{Z}^{V,V}_{N_V\times N_V}\cdot\mathbf{I}^V_{N_V} = \mathbf{0} \tag{16}$$

Combining (14) and (16), all current coefficients can be solved.

$$\begin{bmatrix} \mathbf{Z}^{S,S}_{N'_S\times N_S} & \mathbf{Z}^{S,V}_{N'_S\times N_V} \\ \mathbf{Z}^{V,S}_{N_V\times N'_S} & \mathbf{Z}^{V,V}_{N_V\times N_V} \end{bmatrix} \begin{bmatrix} \mathbf{I}^S_{N'_S} \\ \mathbf{I}^S_{N_V} \end{bmatrix} = \begin{bmatrix} \mathbf{0} - \mathbf{Z}^{S,P}_{N'_S\times N_p}\cdot\mathbf{I}^P_{N_P} \\ \mathbf{0} - \mathbf{Z}^{V,P}_{N_V\times N_p}\cdot\mathbf{I}^P_{N_P} \end{bmatrix} \tag{17}$$

For the voltage source, all unknowns can be directly calculated by solving Equation (11). By combining (11) and (17), the unknowns of the VSIE excited by a finite-gap mixed source can be obtained. In this work, the VSIE matrix equation is solved via iterative solvers, and the associated matrix-vector product can be expressed by

$$\mathbf{Z}\cdot\mathbf{I} = \mathbf{Z}_{\text{Near}}\cdot\mathbf{I} + \mathbf{Z}_{\text{Far}}\cdot\mathbf{I} \tag{18}$$

In (18), $\mathbf{Z}_{\text{Near}}$ is the near-matrix, which is computed using the normal MoM approach. To improve the computational efficiency of VSIE with the finite-gap sources, the second term $\mathbf{Z}_{\text{Far}}\cdot\mathbf{I}$ is accelerated by the MLFMA-MLACEA [20]. Moreover, a robust SAI preconditioner [23] is also used to further accelerate the iterative solution process.

## 3. RESULT

In this section, we first validate the accuracy of the proposed method; its capability is then demonstrated in Sections 3.1 through 3.3. All the simulations are performed on a workstation with Intel(R) Core (TM) i7-8700@3.20 GHz, and 64 GB RAM, and the system equation is solved using the generalized minimal residual algorithm (GMRES).

To illustrate the accuracy of the proposed VSIE scheme, we measure the accuracy by the mean percentage errors (MPEs) of the input impedance, i.e.,

$$\delta(\%) = \frac{1}{N_a}\left(\sum_{i=1}^{N_a}\frac{|Z_{cal,i} - Z_{ref,i}|}{|Z_{ref,i}|}\times 100\%\right) \tag{19}$$

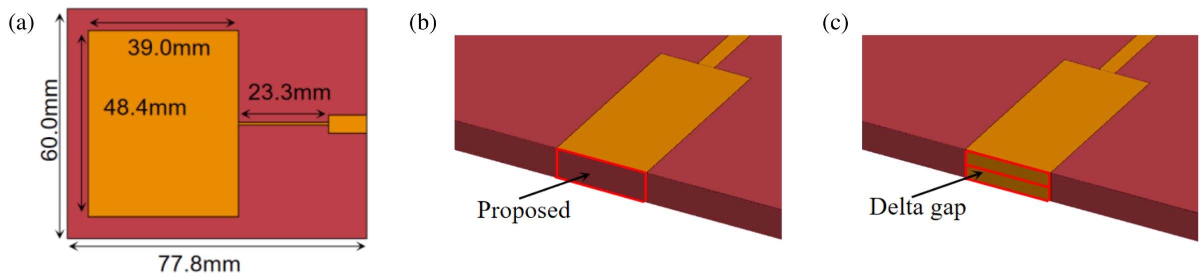


**FIGURE 3.** Microstrip patch antenna. (a) Geometry of this microstrip patch antenna, (b) the finite-gap model, and (c) the traditional delta-gap model.

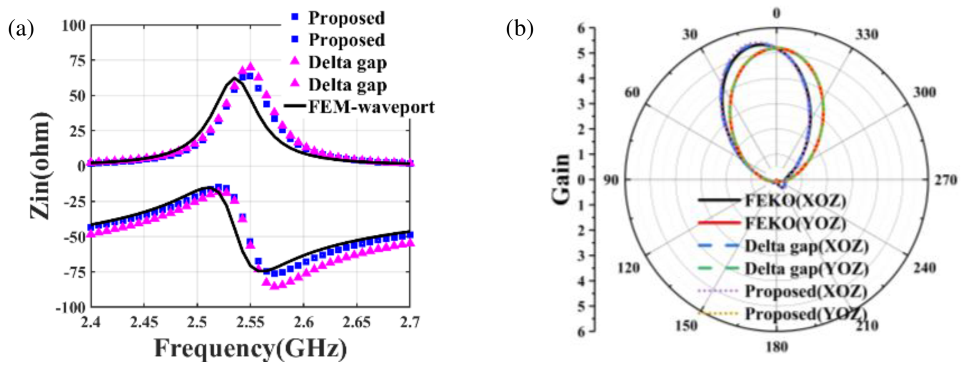


**FIGURE 4.** Input impedance and gain of microstrip patch antenna. (a) Input impedance (Reference impedance = 50 Ω) and (b) comparison of gain at 2.55 GHz.

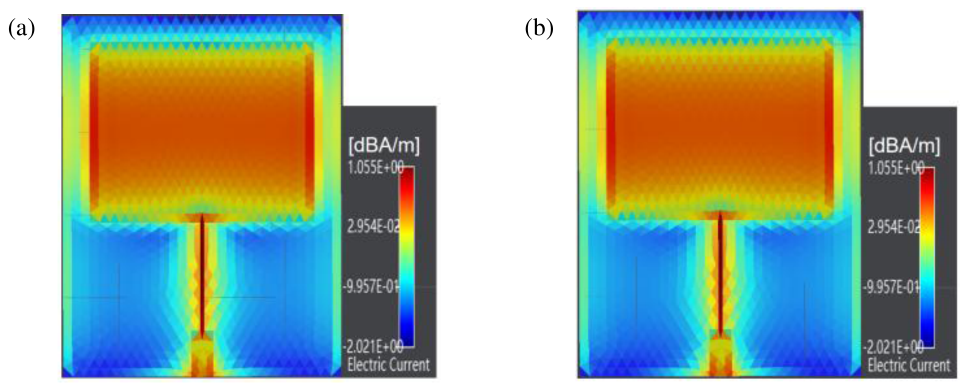


**FIGURE 5.** Illustration of the induced electric current $|\mathbf{J}_S(r)|$ on the surface of the metallic patch at 2.555 GHz. (a) VSIE with the finite-gap model and (b) VSIE with the traditional delta-gap model.

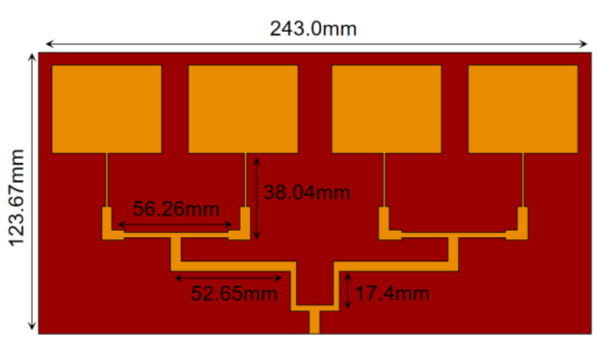


**FIGURE 6.** Geometry of Wilkson microstrip antenna array.

where $Z_{cal,i}$ denotes the input impedance calculated by VSIE, and $Z_{ref,i}$ is the reference result obtained either by the commercial software High Frequency Structure Simulator (HFSS) with finite element method (FEM)-waveport or FEKO. Both $Z_{cal,i}$ and $Z_{ref,i}$ are in ohms. $N_a$ is the number of sampling points.

### 3.1. Microstrip Patch Antenna

The first structure is a single-port, side-fed microstrip patch antenna with a dielectric layer ($\varepsilon_r = 2.20$, $h = 1.575$ mm). Fig. 3(a) shows the dimensions of the antenna. The VSIE-MLFMA-MLACEA discretized by the RWG and SWG basis produces $N'_S = 4630$, $N_V = 16017$ and $N_{port} = 4$. The number of layers for the MLFMA is 5 and for the MLACEA is 4, with a 4th-order expansion.

Figure 4(a) compares the input impedance of the three models, i.e., the proposed finite-gap model, the conventional delta-gap model, and the FEM wave port model, over a frequency

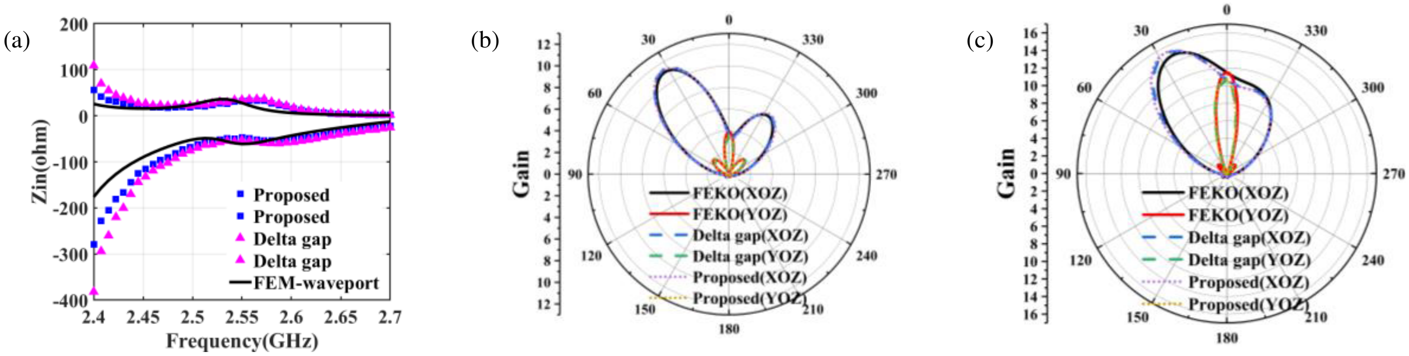


**FIGURE 7**. Input impedance and gain of this Wilkson microstrip antenna array. (a) Input impedance (Reference impedance = 50 Ω), (b) comparison of gain at 2.40 GHz, and (c) comparison of gain at 2.55 GHz.

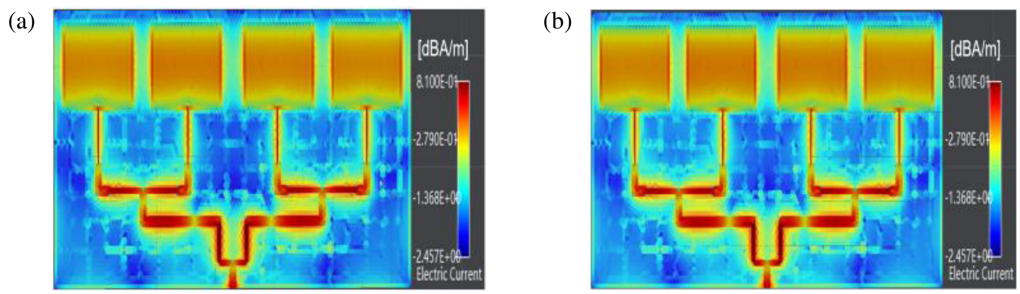


**FIGURE 8**. Illustration of the induced electric current $|\mathbf{J}_S(r)|$ on the surface of the metallic patch at 2.55 GHz. (a) VSIE with the finite-gap model and (b) VSIE with the traditional delta-gap model.

range of approximately $0.3$ GHz. The results from the wave port and the proposed port model agree closely with each other, whereas those from the delta-gap model show significant discrepancies. Note that the input impedance MPE $\delta$ is 4.1% for the proposed port while the MPE for the conventional delta-gap is 4.7%. Fig. 4(b) compares the gain of the three models in the $E$-plane and $H$-plane at $2.55$ GHz, and the results are very similar. Additionally, Fig. 5 shows the induced electric surface currents $|\mathbf{J}_S|$ on the metallic patch for the delta-gap and proposed models, which also agree well with each other.

### 3.2. Wilkinson Microstrip Antenna Array

This example is a 1-port Wilkinson microstrip antenna array $(4 \times 1)$ with a dielectric layer ($\epsilon_r = 2.2$, $h = 1.575$ mm). As can be seen in Fig. 6, a feed network has been added to the linear array. The number of layers for MLFMA is 5 and for MLACEA is 4, with a fifth-order expansion. With the help of the MLFMA-MLACEA, there are 107,134 unknowns, 6.18 GB memory requirements, and 2760 s computational time. Besides, it should be noted that the conventional VSIE-MoM may result in about 29.3 GB memory requirements. The calculated input impedance and gain for the three models are compared over the 2.4–2.7 GHz range in Fig. 7. A 1 V source is placed across the gap between each pair of basis functions, and the port reference impedance is 50 Ω. From these comparisons, we can see that the results obtained with the proposed model in Fig. 7(a) are closer to those of the waveport model than to those of the delta-gap model. For the solution-accuracy comparison, the input impedance MPE is $\delta = 5.2\%$ for the proposed port, versus 6.3% for the conventional delta-gap. The gains at several frequencies are compared in Figs. 7(b) and 7(c), and good agreement is again observed. The current distributions obtained with the delta-gap and the proposed model are presented in Fig. 8.

### 3.3. Helicopter with Monopole Antenna

Figure 9(a) shows a metallic helicopter model with two monopole antennas and a dielectric cabin ($\epsilon_r = 4.4$). The two monopole antennas are located above the helicopter head and above the middle of the tail. For the port discretized by a pair of half-RWG basis functions ($N_{port} = 1$) at 200 MHz, the helicopter is discretized into 47,540 triangles and 20,923 tetrahedra. In this case, the VSIE-MLFMA-MLACEA is adopted, where the number of layers for MLFMA is 8 and for MLACEA is 7, with a fifth-order expansion. There are 117,207 unknowns, 4.76 GB memory requirements, and 6950 s computational time, while the conventional VSIE-MoM with the same discretization results in about 39 GB memory requirements. In this case, benefiting from the SAI preconditioning technique for accelerating the MLFMA-MLFMA algorithm, the GMRES method requires only 274 iterations to solve the matrix equation at a threshold of 0.001. Without preconditioning, the residual drops to only 0.15 after 550 iterations, clearly indicating a significant enhancement in iterative performance.

Three additional cases are considered for the same helicopter, differing in port discretization and frequency. In the first case, the port is discretized using one pair of half-RWG basis functions ($N_{port} = 1$) at 300 MHz, yielding 92,754 triangles and 70,297 tetrahedrons. In the second case, the port is discretized

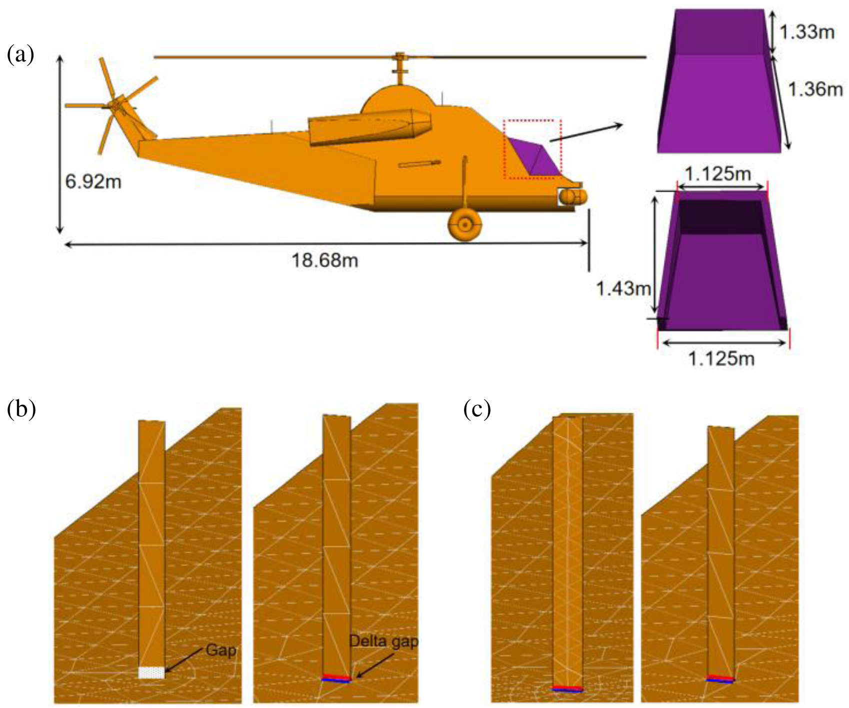


**FIGURE 9**. A helicopter with two monopole antennas. (a) The dimension of this structure, (b) the finite-gap model ($h_{gap} = 0.01$ m) and the traditional delta-gap model, and (c) the finite-gap model discretized by half-RWG basis functions with $N_{port} = 1$ and $N_{port} = 2$.

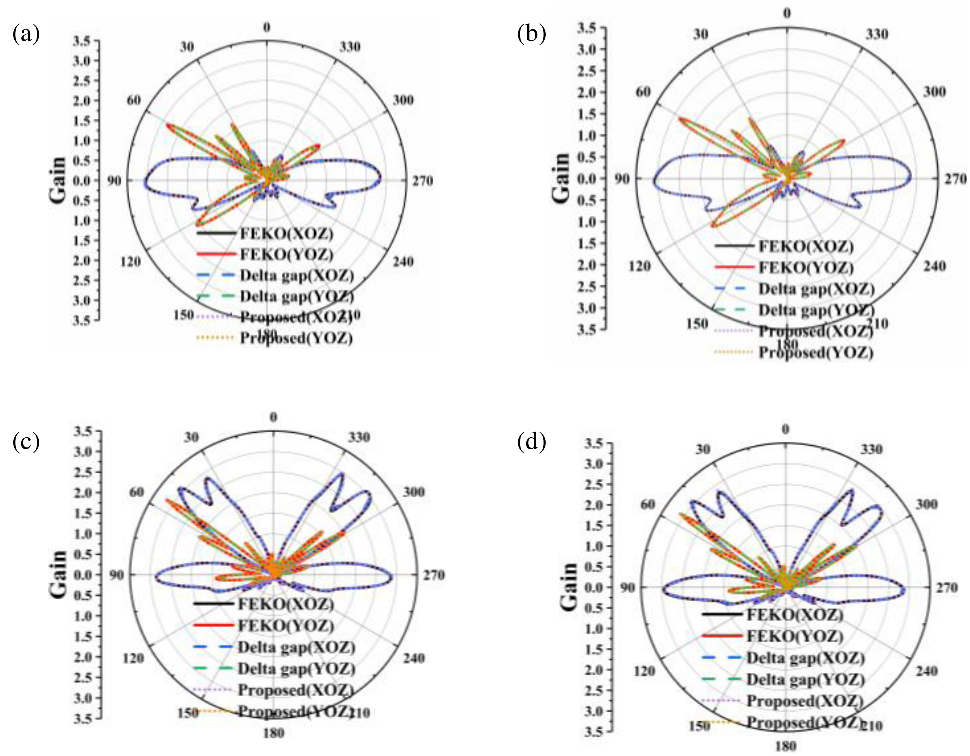


**FIGURE 10**. Comparison of gains. (a) At 200 MHz, $N_m = 1$, (b) at 200 MHz, $N_{port} = 2$, (c) at 300 MHz, $N_{port} = 1$, and (d) at 300 MHz, $N_{port} = 2$.

using two pairs of half-RWG basis functions ($N_{port} = 2$) at 200 MHz, yielding 47,792 triangles and 20,923 tetrahedrons. In the third case, the port is discretized using two pairs of half-RWG basis functions ($N_{port} = 2$) at 300 MHz, yielding 92,956 triangles and 70,297 tetrahedrons.

As summarized in Table 1, the input impedance obtained from the proposed method agrees relatively well with that from FEKO. These results demonstrate the accuracy of the finite-gap model. In Fig. 10, the results from the finite-gap model, conventional delta-gap model, and FEKO are almost identi-

(a) (b) (c) (d)

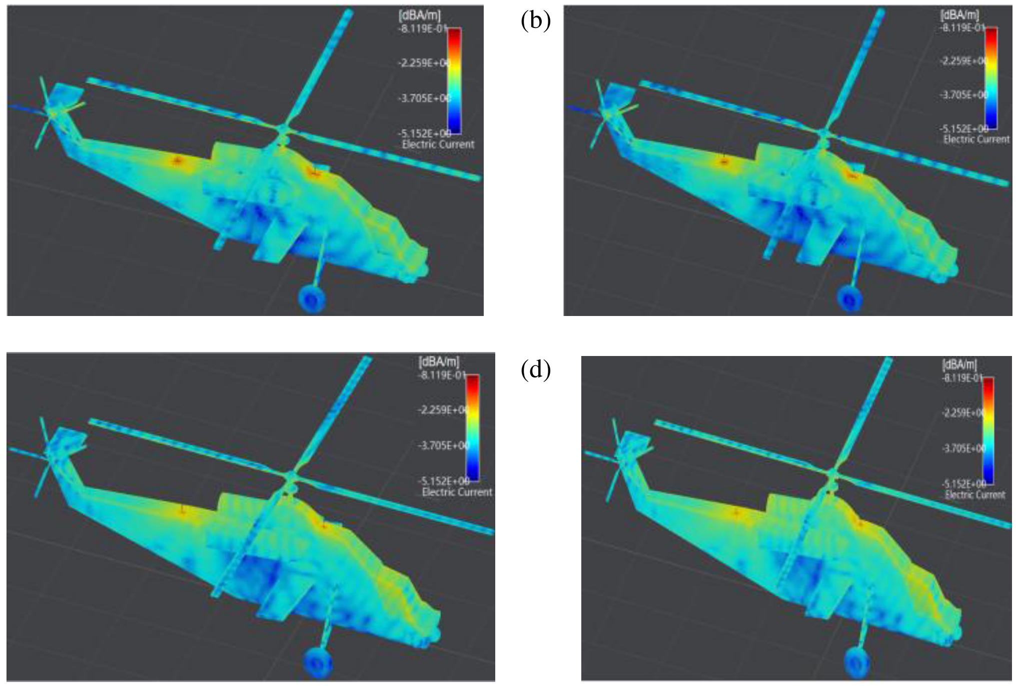


**FIGURE 11**. Illustration of the induced electric current $|J_s(r)|$ on the surface of the metallic patch. (a) VSIE with the finite-gap model at 200 MHz, (b) VSIE with the traditional delta-gap model at 200 MHz, (c) VSIE with the finite-gap model at 300 MHz, and (d) VSIE with the traditional delta-gap model at 300 MHz.

**TABLE 1**. Comparison of input impedance of a helicopter with two monopole antennas

| Frequency | 200 MHz | | 300 MHz | |
|---|---|---|---|---|
| $N_{port}$ | 1 | 2 | 1 | 2 |
| VSIE with conventional delta-gap | 161.0+j166.4 Ω | 284.9+j120.1 Ω | 95.0-j163.1 Ω | 55.6-j137.6 Ω |
| VSIE with finite-gap model | 163.5+j172.3 Ω | 286.5+j130.3 Ω | 108.8-j174.4 Ω | 59.9-j144.9 Ω |
| FEKO | 153.4+j169.4 Ω | 275.8+j126.7 Ω | 104.9-j169.3 Ω | 57.2-j140.7 Ω |

cal. Fig. 11 shows the induced electric currents on the metallic surface for the conventional delta-gap and the proposed finite model. Good agreement is observed. This demonstrates the accuracy, efficiency, and flexibility of the VSIE with the finite-gap model for radiation problems from electrically large and multiscale structures.

## 4. CONCLUSION

A finite-gap model based on VSIE is presented to analyze the radiation from composite metallic and dielectric, electrically large, and multi-scale structures. Different from previous studies on delta-gap, our novel scheme eliminates the redundant metallic patch of the traditional delta-gap model and improves the accuracy of $S$-parameter calculations. Different from this finite-gap lumped-port model for pure metallic structures [17, 18], this model is applied to the VSIE for the first time. Given that VSIE has a broader range of applicability, this extension is both important and valuable. Moreover, a hybrid MLFMA-MLACEA is adopted to enhance the capability of this VSIE with a finite-gap lumped-port model. Numerical results are provided to demonstrate the accuracy and efficiency of this VSIE method.

Further, adopting curved tetrahedral elements and curved triangular patches for geometric modeling and the associated higher-order hierarchical vector (HOHV) basis functions [16] for volume/surface current modeling into this VSIE, much less memory and computational time for the same accuracy level will be achieved for applications in real life where the targets are generally large and multi-scale.

## ACKNOWLEDGEMENT

This work was supported by the National Natural Science Foundation of China under Grants No. 61801406; in part by the Sichuan Provincial Special Project for Central Government Guiding Local Science and Technology Development under Grant No. 2025ZYD0013; in part by the Mianyang Central Guiding Local Science and Technology Development Fund Project under Grants No. 202502ZYDF039, No. 202502ZYDF037 and No. 202502ZYDF008.

## REFERENCES


[1] Ling, F., C.-F. Wang, and J.-M. Jin, "An efficient algorithm for analyzing large-scale microstrip structures using adaptive integral method combined with discrete complex-image method," *IEEE Transactions on Microwave Theory and Techniques*, Vol. 48, No. 5, 832–839, May 2000.

[2] Lo, Y. H., L. J. Jiang, and W. C. Chew, "Finite-width feed and load models," *IEEE Transactions on Antennas and Propagation*, Vol. 61, No. 1, 281–289, Jan. 2013.

[3] Lin, H., T. Li, L. Wang, J. Zhuo, M. Zhuang, and Q. H. Liu, "Efficient electromagnetic simulation of microstrip circuits with uniaxial substrates using the method of moments," *IEEE Transactions on Microwave Theory and Techniques*, Vol. 74, No. 5, 4069–4079, May 2026.

[4] Braaten, B. D. and R. M. Nelson, "An RGF delta-gap source for thin-wire EFIE," *IEEE Transactions on Electromagnetic Compatibility*, Vol. 50, No. 1, 212–215, Feb. 2008.

[5] Liu, T., Y.-W. Zhao, Y.-T. Zheng, and M.-M. Jia, "Accurate computation of input admittance of the antennas on the platform using the advanced delta-gap source model," in *CSQRWC 2012*, 30–34, New Taipei City, 2012.

[6] Young, J. C. and S. D. Gedney, "A delta gap source for locally corrected Nyström discretized integral equations," in *2015 IEEE International Symposium on Antennas and Propagation & USNC/URSI National Radio Science Meeting*, 965–966, Vancouver, BC, Canada, 2015.

[7] Ding, W., G. Wang, F. Liang, and B. Yuan, "An enhanced gap source model," *IEEE Transactions on Antennas and Propagation*, Vol. 61, No. 3, 1266–1272, Mar. 2013.

[8] Trintinalia, L. C., "Simple excitation model for coaxial driven monopole antennas," *IEEE Transactions on Antennas and Propagation*, Vol. 58, No. 6, 1907–1912, Jun. 2010.

[9] Rao, S., D. Wilton, and A. Glisson, "Electromagnetic scattering by surfaces of arbitrary shape," *IEEE Transactions on Antennas and Propagation*, Vol. 30, No. 3, 409–418, May 1982.

[10] Huang, W.-F., Y. Ren, and Q. H. Liu, "Solid-angle error in the magnetic-field integral equation for perfectly electric conducting objects," *IEEE Transactions on Antennas and Propagation*, Vol. 64, No. 3, 1158–1163, Mar. 2016.

[11] Cai, Q.-M., C. Zhang, Y.-W. Zhao, W.-F. Huang, R. Zhang, Z.-P. Zhang, L. Wu, Y.-Y. Zhu, X. Cao, Y. Yu, and Q. H. Liu, "SIE-DDM with higher order hierarchical vector basis functions for solving electromagnetic problems on multiscale metallic targets," *IEEE Transactions on Antennas and Propagation*, Vol. 69, No. 10, 6587–6599, Oct. 2021.

[12] Schaubert, D., D. Wilton, and A. Glisson, "A tetrahedral modeling method for electromagnetic scattering by arbitrarily shaped inhomogeneous dielectric bodies," *IEEE Transactions on Antennas and Propagation*, Vol. 32, No. 1, 77–85, Jan. 1984.

[13] Cai, Q.-M., Z.-P. Zhang, Y.-W. Zhao, W.-F. Huang, Y.-T. Zheng, Z.-P. Nie, and Q. H. Liu, "Nonconformal discretization of electric current volume integral equation with higher order hierarchical vector basis functions," *IEEE Transactions on Antennas and Propagation*, Vol. 65, No. 8, 4155–4169, Aug. 2017.

[14] Yuan, N., T. S. Yeo, X.-C. Nie, Y.-B. Gan, and L.-W. Li, "Analysis of probe-fed conformal microstrip antennas on finite grounded substrate," *IEEE Transactions on Antennas and Propagation*, Vol. 54, No. 2, 554–563, Feb. 2006.

[15] Lu, C. C. and W. C. Chew, "A coupled surface-volume integral equation approach for the calculation of electromagnetic scattering from composite metallic and material targets," *IEEE Transactions on Antennas and Propagation*, Vol. 48, No. 12, 1866–1868, Dec. 2000.

[16] Cai, Q.-M., Y.-W. Zhao, W.-F. Huang, Y.-T. Zheng, Z.-P. Zhang, Z.-P. Nie, and Q. H. Liu, "Volume surface integral equation method based on higher order hierarchical vector basis functions for em scattering and radiation from composite metallic and dielectric structures," *IEEE Transactions on Antennas and Propagation*, Vol. 64, No. 12, 5359–5372, Dec. 2016.

[17] Liu, C., J. W. Massey, and A. E. Yılmaz, "A nonradiating finite-gap lumped-port model," *IEEE Antennas and Wireless Propagation Letters*, Vol. 17, No. 7, 1339–1343, Jul. 2018.

[18] Jia, Y.-R., Q.-M. Cai, Z.-Q. Wu, X. Cao, L. Zhou, H. Li, Z.-Y. Du, Y. Li, Y. Zhu, Y.-T. Zheng, B. Pu, and J. Fan, "A finite-gap port model in SIE with CRWG basis functions for radiation analysis," in *2024 Photonics & Electromagnetics Research Symposium (PIERS)*, 1–5, Chengdu, China, 2024.

[19] Ergul, O. and L. Gurel, "Efficient parallelization of the multilevel fast multipole algorithm for the solution of large-scale scattering problems," *IEEE Transactions on Antennas and Propagation*, Vol. 56, No. 8, 2335–2345, Aug. 2008.

[20] Wu, L., Y. Zhao, Q. Cai, R. Zhang, L. Gu, Z. Zhang, and Z. Nie, "MLACE-MLFMA combined with reduced basis method for efficient wideband electromagnetic scattering from metallic targets," *IEEE Transactions on Antennas and Propagation*, Vol. 67, No. 7, 4738–4747, Jul. 2019.

[21] Wu, L., Y. Zhao, Q. Cai, Z. Zhang, and J. Hu, "An adaptive segmented reduced basis method for fast interpolating the wideband scattering of the dielectric-metallic targets," *IEEE Antennas and Wireless Propagation Letters*, Vol. 19, No. 12, 2235–2239, Dec. 2020.

[22] Cai, Q.-M., Y.-W. Zhao, Y.-T. Zheng, M.-M. Jia, Z. Zhao, and Z.-P. Nie, "Volume integral equation with higher order hierarchical basis functions for analysis of dielectric electromagnetic scattering," *IEEE Transactions on Antennas and Propagation*, Vol. 63, No. 11, 4964–4975, Nov. 2015.

[23] Cai, Q.-M., Y.-W. Zhao, Y.-T. Zheng, L. Gu, Z.-P. Zhang, Z.-P. Nie, W.-F. Huang, and Q. H. Liu, "Higher order multilevel fast multipole algorithm solution of volume integral equation for dielectric electromagnetic scattering," in *2018 IEEE International Conference on Computational Electromagnetics (ICCEM)*, 1–3, Chengdu, China, 2018.